Editors' Suggestion | Featured in Physics

Extreme Domain Wall Speeds under Ultrafast Optical Excitation

Rahul Jangid,[1,2] Nanna Zhou Hagström,[3,1] Meera Madhavi,[1] Kyle Rockwell,[4] Justin M. Shaw,[5] Jeffrey A. Brock,[6] Matteo Pancaldi,[7] Dario De Angelis,[7] Flavio Capotondi,[7] Emanuele Pedersoli,[7] Hans T. Nembach,[8,9] Mark W. Keller,[5] Stefano Bonetti,[3,10] Eric E. Fullerton,[6] Ezio Iacocca,[4] Roopali Kukreja,[1,*] and Thomas J. Silva[5,†]

[1]*Department of Materials Science and Engineering, University of California Davis, Davis, California, USA*
[2]*National Synchrotron Light Source II, Brookhaven National Laboratory, Upton, New York 11973, USA*
[3]*Department of Physics, Stockholm University, 106 91 Stockholm, Sweden*
[4]*Center for Magnetism and Magnetic Nanostructures, University of Colorado Colorado Springs, Colorado Springs, Colorado, USA*
[5]*Quantum Electromagnetics Division, National Institute of Standards and Technology, Boulder, Colorado, USA*
[6]*Center for Memory and Recording Research, University of California San Diego, La Jolla, California, USA*
[7]*Elettra Sincrotrone Trieste S.C.p.A., Area Science Park, S.S. 14 km 163.5, 34149 Trieste, Italy*
[8]*Department of Physics, University of Colorado, Boulder, Colorado 80309, USA*
[9]*Associate, Physical Measurement Laboratory, National Institute of Standards and Technology, Boulder, Colorado 80305, USA*
[10]*Department of Molecular Sciences and Nanosystems, Ca' Foscari University of Venice, 30172 Venezia, Italy*

(Received 28 April 2023; revised 5 July 2023; accepted 8 November 2023; published 19 December 2023)

Time-resolved ultrafast EUV magnetic scattering was used to test a recent prediction of > 10 km/s domain wall speeds by optically exciting a magnetic sample with a nanoscale labyrinthine domain pattern. Ultrafast distortion of the diffraction pattern was observed at markedly different timescales compared to the magnetization quenching. The diffraction pattern distortion shows a threshold dependence with laser fluence, not seen for magnetization quenching, consistent with a picture of domain wall motion with pinning sites. Supported by simulations, we show that a speed of ≈ 66 km/s for highly curved domain walls can explain the experimental data. While our data agree with the prediction of extreme, nonequilibrium wall speeds locally, it differs from the details of the theory, suggesting that additional mechanisms are required to fully understand these effects.

DOI: 10.1103/PhysRevLett.131.256702

The ability to manipulate mesoscopic-scale magnetization [1] has potential applications in ultralow power magnetic memory and logic [2–4]. For example, current-driven domain wall speeds greater than 5 km/s have been demonstrated with bilayers composed of a compensated ferrimagnet and Pt [3]. Exceeding these current-driven domain wall speeds is dependent either on future material breakthroughs or developing novel routes for controlling magnetic behavior. Far-from-equilibrium physics [5,6] in ultrafast conditions [7–9] offers a unique possibility due to the introduction of novel dissipative pathways that are not accessible under equilibrium. In fact, a recent theoretical study by Baláž *et al.* [10] predicts that extremely fast domain wall speeds of ≈ 14 km/s in ferromagnets can be achieved via optical pumping due to superdiffusive spin currents [11]. This is a remarkable prediction as it exceeds the accepted maximum domain-wall speed for ferromagnets, ≈ 400–600 m/s [12–14]. Domain walls, which can be considered as bound magnetic solitons (localized nonlinear excitations with finite energy) [15], undergo Walker breakdown above these speeds, and the solitonlike structure of a domain wall becomes unstable [16,17]. This would imply that ultrafast spin dynamics not only result in an overall demagnetization but can also affect the long-range spatial structure of magnetic domains over several tens of nanometers.

While ultrafast demagnetization is well established for a wide variety of ferromagnetic materials [18,19], only a few studies have hinted toward the ultrafast modification of a nanoscale domain pattern [20–23]. These studies have used x-ray magnetic scattering to show that the diffraction rings obtained from a labyrinthine domain pattern undergo ultrafast distortions of both ring radius and width. Tentative explanations have included domain wall broadening [20,24], and the ultrafast rearrangement of domains [21,22]. While these studies cannot clearly explain ultrafast distortions of diffraction patterns, domain rearrangement remains a viable hypothesis.

To test the prediction of extreme-speed wall motion, we conducted optical pump, EUV magnetic scattering probe experiments with a mixed-state domain pattern that consists of domains of both labyrinthine and stripelike character. Scattering from such samples yields two dominant diffraction components: an azimuthally uniform and a twin-lobed ring pattern [22]. We employed 2D fits similar to those in Zhou Hagström *et al.* [22] to isolate and study the magnetization dynamics of domains of differing character. We measured the pump fluence dependence over an order of magnitude. Given that domain walls typically exhibit both inertia [25,26] and an activation energy barrier, i.e., pinning [17,27], the fluence dependence for the

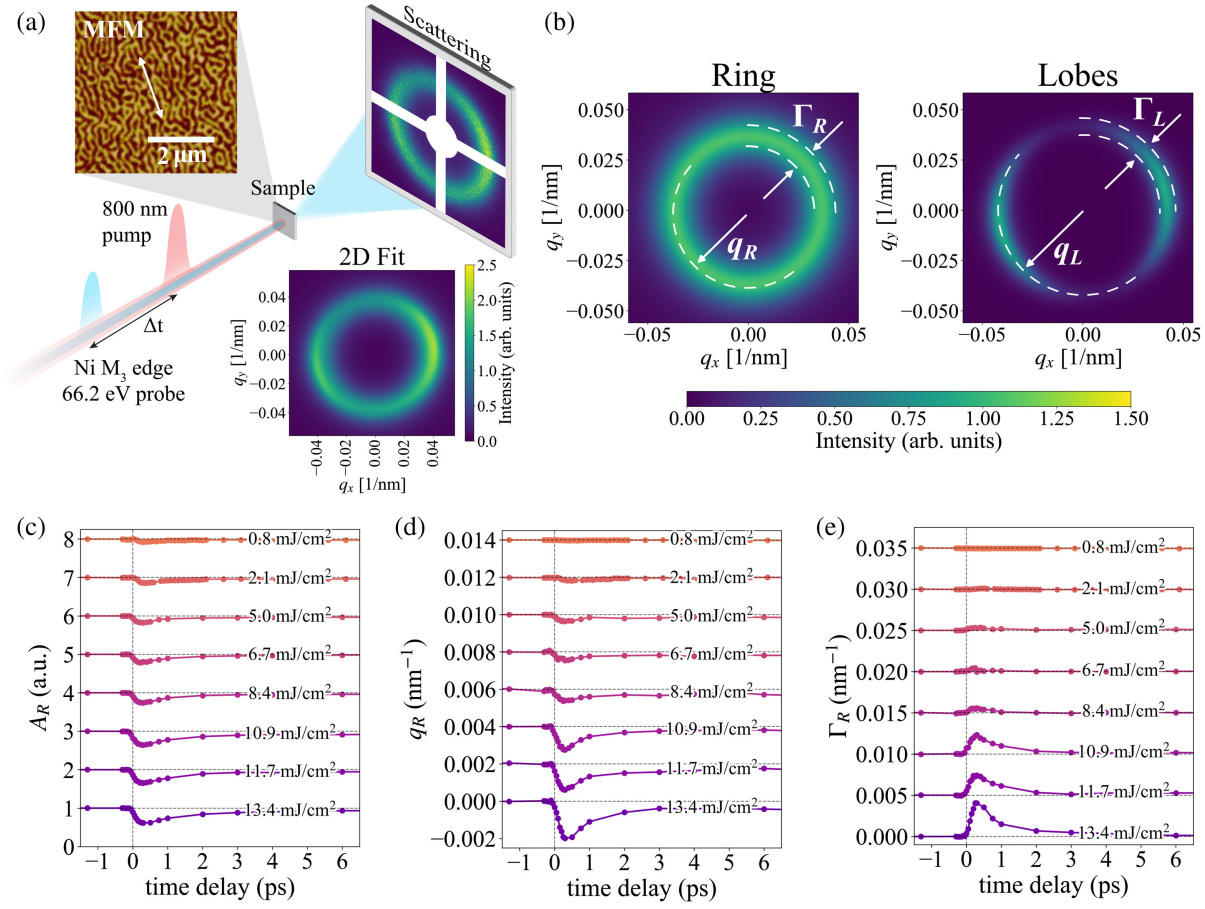

FIG. 1. Experimental schematic and evolution of labyrinthine domain pattern as a function of delay time. (a) Optical pump EUV magnetic scattering probe setup with MFM image of the sample. The white arrow highlights the direction of the linear texture of the domain pattern. Magnetic diffraction scattering on the CCD is fitted with a 2D phenomenological model described in the Supplemental Material Sec. A [28], from which we separate the ring and lobe components. (b) Isolated isotropic (ring) and anisotropic (lobes) fit components with arrows indicating the radius (q_R, q_L) and full-width half maximum (Γ_R, Γ_L) of scattering. Time-resolved (c) amplitude (A_R), (d) ring radius (q_R), and (e) width (Γ_R) obtained from the fit of the isotropic scattering (ring). Delay curves are plotted for a range of measured fluence values from 0.8 to 13.4 mJ/cm^2. The scattering amplitude which is proportional to magnetization, decays immediately following laser excitation indicating demagnetization which recovers on ps timescales. The ring radius (q_R) and width (Γ_R) of the isotropic scattering approximate the average real-space domain size and correlation length of the labyrinthine domains, respectively. Note that the plotted data for A_R, q_R and Γ_R are relative to the before t = 0 value.

ultrafast distortion should be different from that of demagnetization if the ultrafast distortion is the result of domain-wall motion. We employed micromagnetic simulations to test the hypothesis that the preferential motion of curved domain walls in labyrinthine domains is in fact the source of ultrafast distortions. Our results provide experimental evidence for the theoretical proposition that far-from-equilibrium conditions can give rise to extreme domain-wall speeds.

Magnetic resonant scattering was measured by tuning the EUV photon energy to the M_3 edge of Ni at 66.2 eV at the FERMI free electron laser. A schematic of a pump-probe experiment is presented in Fig. 1(a). A magnetic multilayered sample with stack layering of $\{Ta(3\,nm)/Cu(5\,nm)/[Co_{90}Fe_{10}(0.25\,nm)/Ni(1.35\,nm)]\times 8/Co_{90}Fe_{10}(0.25\,nm)/Cu(5\,nm)/Ta(3\,nm)\}$ was used. The sample was grown using magnetron sputtering on 100 nm thick polycrystalline Si membranes and is the same sample as the one used in [22] with average domain width of 110 nm. 50 fs resolution pump-probe measurements were performed with an 800 nm pump and a linearly polarized EUV probe in transmission mode. Note that the nanoscale magnetic domain pattern of the sample exhibits two distinct diffraction features [see Fig. 1(b)]. The first is an isotropic ring attributed to a randomly oriented labyrinth pattern. The second are anisotropic lobes attributed to the stripelike component of the domain pattern. Linear orientation of the labyrinth domains, verified by magnetic force microscope (MFM) [see Fig. 1(a)], was observed due to irreversible laser-induced deformation of the supporting membrane [22]. The resultant strain induced in the supported magnetic multilayer led to a weak in-plane

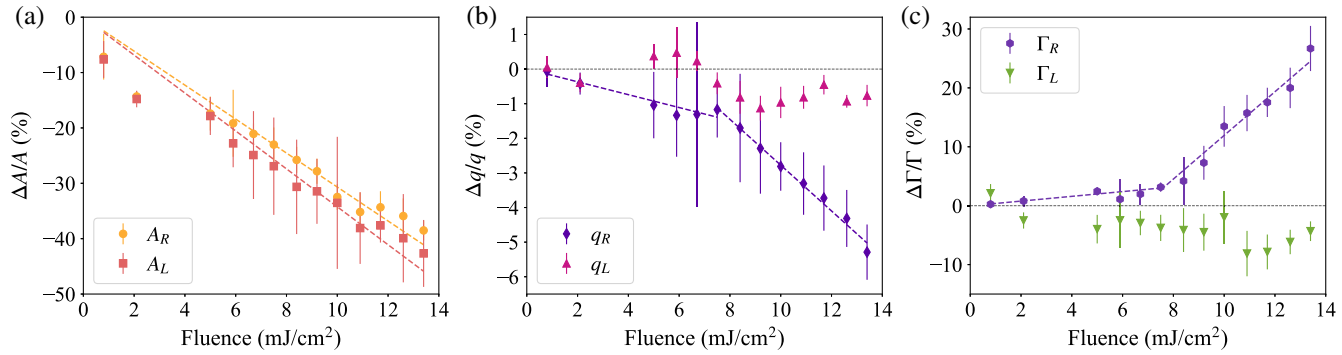

FIG. 2. Laser fluence dependence of isotropic and anisotropic scattering from labyrinthine and stripe domains. (a) Normalized scattered amplitude dependence on fluence for both the isotropic (A_R) and anisotropic scattering (A_L). Fluence dependence of (b) ring shift and (c) width for both the ring ($\Delta q_R/q_R$ and $\Delta\Gamma_R/\Gamma_R$) and lobes ($\Delta q_L/q_L$ and $\Delta\Gamma_L/\Gamma_L$). The dashed lines indicate the results of linear error-weighted fits of the data. For A_R and A_L, the fits extend over the entire range of pump fluence. For $\Delta q_R/q_R$ and $\Delta\Gamma_R/\Gamma_R$, two fits were performed below and above the threshold fluence of 7.8 mJ/cm^2.

component of magnetic anisotropy. In order to isolate the ultrafast behavior of these two features, the scattering data were fitted using a phenomenological 2D model similar to [22]. Fit results including isotropic ring and anisotropic lobe components are also shown in Fig. 1(b). Additional details on the fitting procedure can be found in the Supplemental Material, Sec. A [28], which includes references [29–37].

Figures 1(c)–1(e) show the ultrafast temporal evolution of the isotropic diffraction ring in terms of amplitude A_R, q space radius q_R, and width Γ_R. An ultrafast distortion of the diffraction ring was observed, manifesting as both a reduction in the ring radius, and a broadening of the ring width. The temporal evolution of the equivalent parameters for the anisotropic lobe pattern (A_L, q_L, Γ_L) are presented in Fig. S4 of the Supplemental Material [28]. The demagnetization (A_R and A_L) occurs within 100–200 fs followed by a slower recovery between 400 fs and 1.4 ps, depending on the fluence as further discussed below. A double-exponential fitting function as described in the Supplemental Material, Sec. B [28], was used to extract both magnitudes and time constants associated with the temporal response.

Figure 2 shows the fluence dependence for both the ring and lobes including demagnetization ($\Delta A_R/A_R$, $\Delta A_L/A_L$), radial peak shift ($\Delta q_R/q_R$, $\Delta q_L/q_L$), and ring broadening ($\Delta\Gamma_R/\Gamma_R$, $\Delta\Gamma_L/\Gamma_L$) relative to the average fitted prepump values for $t < 0$. These results are also tabulated in Table S1 in the Supplemental Material [28]. The fluence dependencies of both $\Delta A_R/A_R$ and $\Delta A_L/A_L$ are very similar, and are consistent with most previous pump-probe studies [22]. The nonlinearity of both $\Delta q_R/q_R$ and $\Delta\Gamma_R/\Gamma_R$ seen in Figs. 2(b) and 2(c) is in stark contrast to the linear fluence dependence of the amplitude quenching $\Delta A_R/A_R$ and $\Delta A_L/A_L$ shown in Fig. 2(a). $\Delta q_R/q_R$ and $\Delta\Gamma_R/\Gamma_R$ exhibit a distinct thresholdlike feature. For fluences below 7 mJ/cm^2, a relatively weak linear dependence of both $\Delta q_R/q_R$ and $\Delta\Gamma_R/\Gamma_R$ on fluence is observed. Above 7 mJ/cm^2, a much steeper linear dependence of $\Delta q_R/q_R$ and $\Delta\Gamma_R/\Gamma_R$ on pump fluence is observed, with $\Delta q_R/q_R = 5.3 \pm 0.8\%$ and $\Delta\Gamma_R/\Gamma_R = 26.7 \pm 3.8\%$ at the highest fluence. In contrast, $\Delta q_L/q_L$ and $\Delta\Gamma_L/\Gamma_L$ are much smaller and without any apparent linear dependence on fluence, with largest observed shifts of $1.0 \pm 0.4\%$ and $8.1 \pm 3.8\%$, respectively. The thresholdlike behavior of the ultrafast diffraction ring distortions is the first main experimental result of this Letter.

Time constants for the initial ultrafast changes τ_m and slower recovery τ_{rec} for A_R, A_L, q_R, and Γ_R are presented in Fig. 3. The demagnetization times for both the ring and lobes vary between 100 and 200 fs, indicative of a similar demagnetization process for labyrinths and stripes. Surprisingly, the time constants τ_m for the change in ring radius and ring width vary between 100 and 300 fs, with most data falling between 200 and 300 fs, significantly slower than the demagnetization times. In addition, the recovery times τ_{rec} are also different between the demagnetization and ring shape distortions. The demagnetization recovery times vary from ≈600 fs to ≈1.2 ps, whereas both the ring radius and width recover much faster, with most data falling between 200 fs and 600 fs, dependent on the fluence. This difference in temporal response for demagnetization and ring distortion is the second key finding of this Letter.

The threshold fluence for ring distortion ($\Delta q_R/q_R$ and $\Delta\Gamma_R/\Gamma_R$ in Fig. 2) suggests that there is an activation energy barrier impeding domain rearrangement as typically observed for conventional field-driven wall dynamics [17]. This result is consistent with the hypothesis that domain rearrangement in the presence of pinning sites is the source of ultrafast ring distortions. Furthermore, the relatively slow rate (Fig. 3) for the change of $\Delta q_R/q_R$ and $\Delta\Gamma_R/\Gamma_R$ is consistent with domain-wall motion. Domain walls are bound magnetic solitons that exhibit an effective inertia [15,25,26] that impedes the response to any driving torque. Thus, based on the distinct response times for demagnetization and the ring distortions, we can confidently rule out

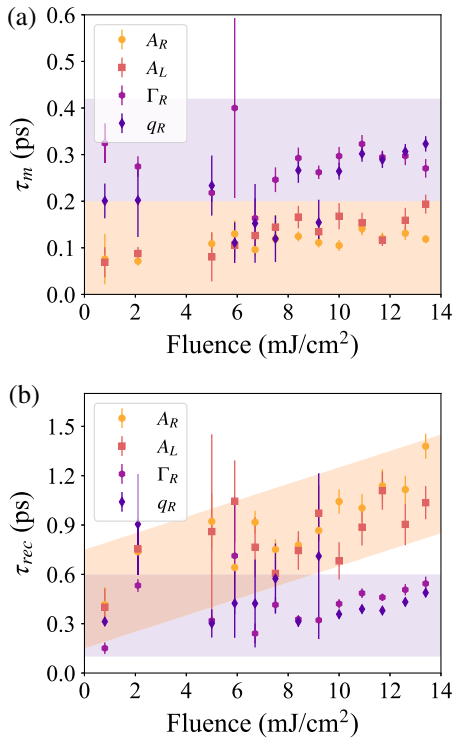

FIG. 3. Laser fluence dependence of quench and recovery time. (a) Quench and (b) recovery time constants obtained from the temporal fits (see the Supplemental Material, Sec. B SM) for A_R, A_L, q_R, and Γ_R. The magnetization quench is 2 times faster than the change in radial ring position and ring width ($\tau_m \approx 0.3$ ps) irrespective of the fluence value. The recovery time constants (τ_{rec}) for magnetization quench (A_R and A_L) are also distinct from τ_{rec} for ring shift (q_R) and width (Γ_R).

any hypothesis that the distortions in diffraction ring shape are simply derivative results of ultrafast demagnetization process.

Given the substantial differences in the ultrafast distortions of the stripe and labyrinth domain pattern, in agreement with the previous report [22], it is natural to inquire what characteristic features of labyrinth and stripe domains underlie such differences in temporal response. An obvious difference is the abundance of curved domain walls for labyrinths. The possibility of curved wall motion, in contrast to that for straight walls, is consistent with the requirement of symmetry breaking. Symmetry breaking was provided in the original prediction of ultrafast wall motion by nonuniform laser illumination of a straight domain wall [10]. In our case, the symmetry breaking is geometrical, inherent in the wall curvature.

To verify whether the spatial motion of curved domain walls can give rise to the observed contraction of the diffraction ring radius, we performed micromagnetic simulations [38] for the case of a perpendicularly magnetized thin film. We used magnetic parameters determined for the same sample in [22]: saturation magnetization $M_s = 616$ kA/m, exchange constant $A = 20$ pJ/m, Gilbert damping constant $\alpha = 0.01$, first-order uniaxial anisotropy $K_1 = 739$ kJ/m^3, and second-order uniaxial anisotropy $K_2 = -266$ kJ/m^3. An initial equilibrium domain state with either labyrinthine or stripelike character was generated. The domain state was then modified by suddenly reducing the saturation magnetization by 40%. The magnetization was allowed to evolve according to conventional micromagnetic parameters to a new equilibrium state. This resulted in substantial domain wall displacements for the labyrinthine sample, where the displacements were proportional to the local domain wall curvature (see the Supplemental Material, Sec. D [28] for additional details). While the timescale for the wall displacement is not accurate due to the use of micromagnetic simulations [39], the dependence of wall displacement on the curvature allows us to examine how such domain rearrangement

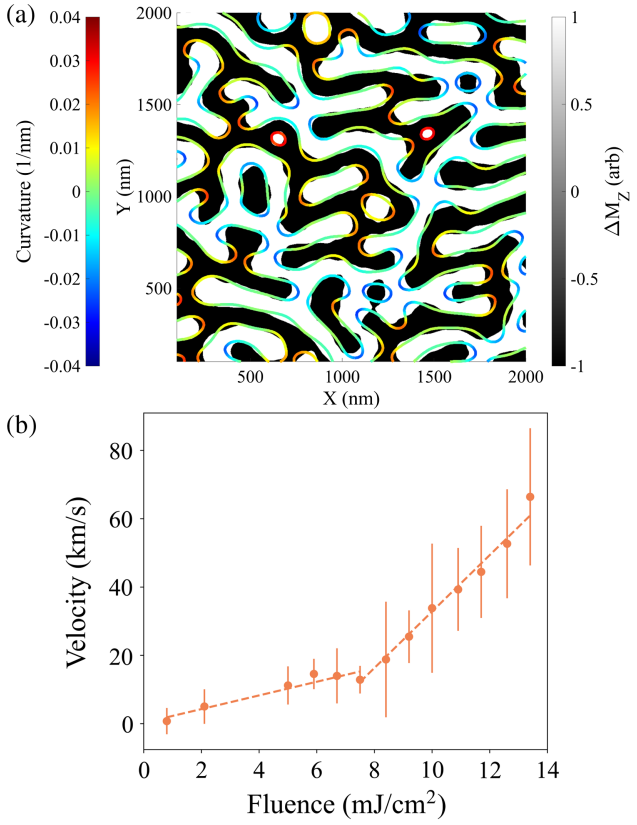

FIG. 4. Simulated modification of domain pattern and calculated domain wall velocity. (a) Simulated modified domain pattern (black and white domains) and initial state (colored outline). The modified state was simulated assuming a 40% reduction in the saturation magnetization as discussed in the text. The color of the outline denotes the initial wall curvature which was estimated using the inverse of the radius of local circle fit. The comparison clearly shows that regions with high curvature (dark red and blue) undergo noticeable domain wall motion. (b) Fluence dependence of calculated domain wall velocity for labyrinthine domains estimated using experimentally measured and simulated contraction of diffraction ring radius.

affects the domain pattern in reciprocal space. Figure 4(a) presents the simulated modified labyrinth domain pattern (black and white domains) and compares it with the initial domain pattern, where only the outline is shown and the color denotes initial wall curvature. The figure clearly shows that domain walls with higher curvature (dark red or blue) undergo noticeable wall motion. Both the observed diffraction ring radius contraction and width broadening were qualitatively reproduced by FFT analysis of the modified simulated labyrinth domain state (see the Supplemental Material, Sec. D [28]). In contrast, the same modeling of a stripe domain pattern with minimal curved walls does not show any detectable distortions in the shape of the FFT spatial pattern (see the Supplemental Material, Fig. S8, [28]).

We can now estimate the domain wall speeds of the curved walls by utilizing both the experimentally measured and simulated contraction of the diffraction ring radius. This was achieved by quantitatively correlating the reduction of diffraction ring radius $[(\Delta q/q)_{\mathrm{sim}}]$ with the modeled change in the wall position by defining parameter $K = (\Delta A_{\mathrm{rms}}/A)/(\Delta q/q)_{\mathrm{sim}}$, where $\Delta A_{\mathrm{rms}}/A$ is fractional areal change due to wall motion. We then determined the average wall displacement necessary to cause the experimentally observed contraction in the diffraction ring radius. The domain wall velocity was calculated using the following equation: $v = K[(\Delta q/q)_{\mathrm{exp}}/\rho_c w \tau_m]$. Here $(\Delta q/q)_{\mathrm{exp}}$ is the experimentally observed fractional change in diffraction ring radius and τ_m is the time constant for the radial shift obtained from temporal fits to the experimental data. K is the proportionality constant as defined above. w is the average domain width, and ρ_c is the curvature density obtained from the MFM images. Additional details on domain wall speed calculations are presented in the Supplemental Material, Sec. E [28]. We can then estimate average domain wall speeds of the curved walls as a function of pump fluence, presented in Fig. 4(b). For 13.4 mJ/cm^2, we estimated rms curve wall displacement to be $\approx 20 \pm 3$ nm, which results in the calculated domain wall speed of 66 ± 20 km/s. The observation of extreme wall speed under far-from-equilibrium conditions is the third and most significant result of this Letter. This is a surprising result since domain walls in ferromagnets near equilibrium are unstable when driven above the Walker limit [16,17].

We note that the observation of threshold effect and distinct time constants of ring distortion and demagnetization indicate that the existing theory is still inadequate to predict the scale of the observed phenomena. The faster rate of distortion recovery suggests more complex physics whereby the relaxation channels for wall dynamics are not identical to those for the demagnetization recovery. It is possible that other mechanisms such as magnon excitation and relaxation need to be included [40–47]. Indeed, the observed temporal response of the wall dynamics is like that of a critically damped oscillator. This suggests that far-from-equilibrium conditions can give rise to new sources of elastic torque that can affect mesoscopic spin textures. Overall, our Letter highlights two critical points for far-from-equilibrium behavior. First, our results show significant evidence of extreme domain wall speeds in qualitative agreement with theoretical predictions [10]. Secondly, most proposed mechanisms for ultrafast demagnetization rely on entropy-producing microscopic single-particle processes which occur on a length scale between the lattice constant and the exchange length. However, extremely fast spatial translation of domain walls requires a long-range mechanism that extends over tens of nanometers, i.e., at the mesoscopic scale [1]. The implication is that far-from-equilibrium spin kinetics in ferromagnets are not solely limited to demagnetization mechanisms.

The raw data generated at FERMI as well as the source code has been made available on Open Science Framework (OSF) [48].

The authors acknowledge the FERMI Free Electron laser in Trieste, Italy for allowing us to use the Diffraction and Projection Imaging (DiProI) beamline and thank the beamline scientists and facility staff for their assistance. R. J., M. M., and R. K. acknowledge support from AFOSR Grant. No. FA9550-19-1-0019. N. Z. H. and S. B. acknowledge support from the European Research Council, Starting Grant No. 715452 MAGNETIC-SPEED-LIMIT. E. I. acknowledges support from the National Science Foundation under Grant No. 2205796. This research was funded by National Institute of Standards and Technology (NIST). The authors acknowledge D. Bozhko for representative experimental data to seed stripe domains in micromagnetic simulations. The identification of specific equipment, instruments, software, or materials in this paper does not imply endorsement by NIST, nor does it indicate their superiority for the intended purpose.

*Corresponding author: rkukreja@ucdavis.edu
†Corresponding author: thomas.silva@nist.gov

[1] L. J. Heyderman, J. Grollier, C. H. Marrows, P. Vavassori, D. Grundler, D. Makarov, and S. Pané, Mesoscopic magnetic systems: From fundamental properties to devices, Appl. Phys. Lett. **119**, 080401 (2021).
[2] S. S. P. Parkin, M. Hayashi, and L. Thomas, Magnetic Domain-Wall Racetrack Memory, Science **320**, 190 (2008).
[3] L. Caretta, M. Mann, F. Büttner, K. Ueda, B. Pfau, C. M. Günther, P. Hessing, A. Churikova, C. Klose, M. Schneider, D. Engel, C. Marcus, D. Bono, K. Bagschik, S. Eisebitt, and G. S. D. Beach, Fast current-driven domain walls and small skyrmions in a compensated ferrimagnet, Nat. Nanotechnol. **13**, 1154 (2018).
[4] A. Manchon, J. Železný, I. M. Miron, T. Jungwirth, J. Sinova, A. Thiaville, K. Garello, and P. Gambardella,

Current-induced spin-orbit torques in ferromagnetic and antiferromagnetic systems, Rev. Mod. Phys. **91**, 035004 (2019).

[5] I. Prigogine, Time, structure and fluctuations, in *Nobel Lectures, Chemistry 1971-1980*, edited by T. Frängsmyr and S. Forsén (World Scientific Publishing Co., Singapore, 1993).

[6] J. Hemminger, G. Fleming, and M. Ratner, Directing matter and energy: Five challenges for science and the imagination, Technical Report No. 935427, U.S. Department of Energy, 2007.

[7] E. G. Tveten, A. Brataas, and Y. Tserkovnyak, Electron-magnon scattering in magnetic heterostructures far out of equilibrium, Phys. Rev. B **92**, 180412(R) (2015).

[8] F. Hellman *et al.*, Interface-induced phenomena in magnetism, Rev. Mod. Phys. **89**, 025006 (2017).

[9] H. Dürr, The x-ray view of ultrafast magnetism, in *Synchrotron Light Sources and Free-Electron Lasers*, edited by E. J. Jaeschke, S. Khan, J. R. Schneider, and J. B. Hastings (Springer International Publishing, Cham, 2016), pp. 1541–1556, 10.1007/978-3-319-14394-1_50.

[10] P. Baláž, K. Carva, U. Ritzmann, P. Maldonado, and P. M. Oppeneer, Domain wall dynamics due to femtosecond laser-induced superdiffusive spin transport, Phys. Rev. B **101**, 174418 (2020).

[11] M. Battiato, K. Carva, and P. M. Oppeneer, Superdiffusive spin transport as a mechanism of ultrafast demagnetization, Phys. Rev. Lett. **105**, 027203 (2010).

[12] M. Schöbitz, A. De Riz, S. Martin, S. Bochmann, C. Thirion, J. Vogel, M. Foerster, L. Aballe, T. O. Menteş, A. Locatelli, F. Genuzio, S. Le-Denmat, L. Cagnon, J. C. Toussaint, D. Gusakova, J. Bachmann, and O. Fruchart, Fast domain wall motion governed by topology and Œrsted fields in cylindrical magnetic nanowires, Phys. Rev. Lett. **123**, 217201 (2019).

[13] I. Lemesh and G. S. D. Beach, Walker breakdown with a twist: Dynamics of multilayer domain Walls and Skyrmions driven by spin-orbit torque, Phys. Rev. Appl. **12**, 044031 (2019).

[14] E. Martinez, S. Emori, N. Perez, L. Torres, and G. S. D. Beach, Current-driven dynamics of Dzyaloshinskii domain walls in the presence of in-plane fields: Full micromagnetic and one-dimensional analysis, J. Appl. Phys. **115**, 213909 (2014).

[15] A. Kosevich, B. Ivanov, and A. Kovalev, Magnetic solitons, Phys. Rep. **194**, 117 (1990).

[16] N. L. Schryer and L. R. Walker, The motion of 180° domain walls in uniform dc magnetic fields, J. Appl. Phys. **45**, 5406 (1974).

[17] J. Ferré, P. J. Metaxas, A. Mougin, J.-P. Jamet, J. Gorchon, and V. Jeudy, Universal magnetic domain wall dynamics in the presence of weak disorder, C.R. Phys. **14**, 651 (2013).

[18] A. Kirilyuk, A. V. Kimel, and T. Rasing, Laser-induced magnetization dynamics and reversal in ferrimagnetic alloys, Rep. Prog. Phys. **76**, 026501 (2013).

[19] S. Jeppson and R. Kukreja, Capturing Ultrafast Magnetization Phenomenon Using Femtosecond x Rays, APL Mater. **9**, 100702 (2021).

[20] B. Pfau *et al.*, Ultrafast optical demagnetization manipulates nanoscale spin structure in domain walls, Nat. Commun. **3**, 1100 (2012).

[21] D. Zusin *et al.*, Ultrafast perturbation of magnetic domains by optical pumping in a ferromagnetic multilayer, Phys. Rev. B **106**, 144422 (2022).

[22] N. Zhou Hagström *et al.*, Symmetry-dependent ultrafast manipulation of nanoscale magnetic domains, Phys. Rev. B **106**, 224424 (2022).

[23] N. Kerber, D. Ksenzov, F. Freimuth, F. Capotondi, E. Pedersoli, I. Lopez-Quintas, B. Seng, J. Cramer, K. Litzius, D. Lacour, H. Zabel, Y. Mokrousov, M. Kläui, and C. Gutt, Faster chiral versus collinear magnetic order recovery after optical excitation revealed by femtosecond XUV scattering, Nat. Commun. **11**, 6304 (2020).

[24] T. Sant, D. Ksenzov, F. Capotondi, E. Pedersoli, M. Manfredda, M. Kiskinova, H. Zabel, M. Kläui, J. Lüning, U. Pietsch, and C. Gutt, Measurements of ultrafast spin-profiles and spin-diffusion properties in the domain wall area at a metal/ferromagnetic film interface, Sci. Rep. **7**, 15064 (2017).

[25] C. Kittel, Note on the inertia and damping constant of ferromagnetic domain boundaries, Phys. Rev. **80**, 918 (1950).

[26] J. Rhensius, L. Heyne, D. Backes, S. Krzyk, L. J. Heyderman, L. Joly, F. Nolting, and M. Kläui, Imaging of domain wall inertia in permalloy half-ring nanowires by time-resolved photoemission electron microscopy, Phys. Rev. Lett. **104**, 067201 (2010).

[27] N. D. Rizzo, T. J. Silva, and A. B. Kos, Relaxation times for magnetization reversal in a high coercivity magnetic thin film, Phys. Rev. Lett. **83**, 4876 (1999).

[28] See Supplemental Material at http://link.aps.org/supplemental/10.1103/PhysRevLett.131.256702 for further details on 2D fitting procedure and time constant fits, comparison of radial shift observed here and literature, details on micromagnetic simulations and domain wall velocity calculations.

[29] S. Valencia, A. Gaupp, W. Gudat, H.-C. Mertins, P. M. Oppeneer, D. Abramsohn, and C. M. Schneider, Faraday rotation spectra at shallow core levels: 3p edges of Fe, Co, and Ni, New J. Phys. **8**, 254 (2006).

[30] J. B. Kortright, M. Rice, and R. Carr, Soft-x-ray Faraday rotation at Fe $L2,3$ edges, Phys. Rev. B **51**, 10240 (1995).

[31] V. Unikandanunni, R. Medapalli, E. E. Fullerton, K. Carva, P. M. Oppeneer, and S. Bonetti, Anisotropic ultrafast spin dynamics in epitaxial cobalt, Appl. Phys. Lett. **118**, 232404 (2021).

[32] A. Axelevitch, B. Gorenstein, and G. Golan, Investigation of optical transmission in thin metal films, Phys. Procedia **32**, 1 (2012).

[33] B. Vodungbo, J. Gautier, G. Lambert, A. B. Sardinha, M. Lozano, S. Sebban, M. Ducousso, W. Boutu, K. Li, B. Tudu, M. Tortarolo, R. Hawaldar, R. Delaunay, V. López-Flores, J. Arabski, C. Boeglin, H. Merdji, P. Zeitoun, and J. Lüning, Laser-induced ultrafast demagnetization in the presence of a nanoscale magnetic domain network, Nat. Commun. **3**, 999 (2012).

[34] M. Hennes, A. Merhe, X. Liu, D. Weder, C. v. K. Schmising, M. Schneider, C. M. Günther, B. Mahieu, G. Malinowski, M. Hehn, D. Lacour, F. Capotondi, E. Pedersoli, I. P. Nikolov, V. Chardonnet, E. Jal, J. Lüning, and B. Vodungbo, Laser-induced ultrafast demagnetization

and perpendicular magnetic anisotropy reduction in a Co88Tb12 thin film with stripe domains, Phys. Rev. B **102**, 174437 (2020).

[35] J. M. Shaw, H. T. Nembach, and T. J. Silva, Measurement of orbital asymmetry and strain in $Co_{90}Fe_{10}$/Ni multilayers and alloys: Origins of perpendicular anisotropy, Phys. Rev. B **87**, 054416 (2013).

[36] L. Caretta, S.-H. Oh, T. Fakhrul, D.-K. Lee, B. H. Lee, S. K. Kim, C. A. Ross, K.-J. Lee, and G. S. D. Beach, Relativistic kinematics of a magnetic soliton, Science **370**, 1438 (2020).

[37] H. A. Mook and D. McK. Paul, Neutron-scattering measurement of the spin-wave spectra for nickel, Phys. Rev. Lett. **54**, 227 (1985).

[38] A. Vansteenkiste, J. Leliaert, M. Dvornik, M. Helsen, F. Garcia-Sanchez, and B. Van Waeyenberge, The design and verification of MuMax3, AIP Adv. **4**, 107133 (2014).

[39] E. Iacocca *et al.*, Spin-current-mediated rapid magnon localisation and coalescence after ultrafast optical pumping of ferrimagnetic alloys, Nat. Commun. **10**, 1756 (2019).

[40] Y. Zhang, T.-H. Chuang, Kh. Zakeri, and J. Kirschner, Relaxation time of terahertz magnons excited at ferromagnetic surfaces, Phys. Rev. Lett. **109**, 087203 (2012).

[41] K. Zakeri, Elementary spin excitations in ultrathin itinerant magnets, Phys. Rep. **545**, 47 (2014).

[42] M. F. Elhanoty, O. Eriksson, R. Knut, O. Karis, and O. Grånäs, Element-selective ultrafast magnetization dynamics of hybrid Stoner-Heisenberg magnets, Phys. Rev. B **105**, L100401 (2022).

[43] G.-M. Choi, B.-C. Min, K.-J. Lee, and D. G. Cahill, Spin current generated by thermally driven ultrafast demagnetization, Nat. Commun. **5**, 4334 (2014).

[44] E. Turgut, D. Zusin, D. Legut, K. Carva, R. Knut, J. M. Shaw, C. Chen, Z. Tao, H. T. Nembach, T. J. Silva, S. Mathias, M. Aeschlimann, P. M. Oppeneer, H. C. Kapteyn, M. M. Murnane, and P. Grychtol, Stoner versus Heisenberg: Ultrafast exchange reduction and magnon generation during laser-induced demagnetization, Phys. Rev. B **94**, 220408(R) (2016).

[45] R. Knut *et al.*, Inhomogeneous Magnon Scattering during Ultrafast Demagnetization, arXiv:1810.10994.

[46] M. Beens, R. A. Duine, and B. Koopmans, $s-d$ model for local and nonlocal spin dynamics in laser-excited magnetic heterostructures, Phys. Rev. B **102**, 054442 (2020).

[47] C. Léveillé *et al.*, Ultrafast time-evolution of chiral Néel magnetic domain walls probed by circular dichroism in x-ray resonant magnetic scattering, Nat. Commun. **13**, 1412 (2022).

[48] R. Jangid, Extreme domain wall speeds under ultrafast optical excitation (2023), 10.17605/OSF.IO/U5XHC.